arXiv:1505.02470v1 [quant-ph] 11 May 2015

Coherent Quantum Control of $S_2 \leftrightarrow S_1$ Internal Conversion in Pyrazine via $S_0 \to S_2/S_1$ Weak Field Excitation

Timur Grinev [1]

Department Of Chemistry, Chemical Physics Theory Group, and Center for Quantum Information and Quantum Control, University of Toronto, Toronto, Ontario M5S 3H6, Canada

Moshe Shapiro

Department of Chemistry and Department of Physics, University of British Columbia, Vancouver, British Columbia V6T 1Z1, Canada, and Department of Chemical Physics, Weizmann Institute of Science, Rehovot 76100, Israel

Paul Brumer

Department Of Chemistry, Chemical Physics Theory Group, and Center for Quantum Information and Quantum Control, University of Toronto, Toronto, Ontario M5S 3H6, Canada

Abstract

Coherent control of internal conversion (IC) between the first (S_1) and second (S_2) singlet excited electronic states in pyrazine, where the S_2 state is populated from the ground singlet electronic state S_0 by weak field excitation, is examined. Control is implemented by shaping the laser which excites S_2. Excitation and IC are considered simultaneously, using the recently introduced resonance-based control approach. Highly successful control is achieved by optimizing both the amplitude and phase profiles of the laser spectrum. The dependence of control on the properties of resonances in S_2 is demonstrated.

I. INTRODUCTION

Coherent quantum control [2, 3] has been extensively studied for a wide variety of systems and proven to be a useful approach to controlling properties of atomic and molecular systems. For example, in bound systems it has been used to suppress spontaneous emission from a manifold of states [4], and to control radiationless transitions in collinear carbonyl sulfide OCS [5] and in pyrazine $C_4H_4N_2$ [6–8].

Christopher et al. examined [6, 8] radiationless transitions in pyrazine from the S_2 to the S_1 electronic state and controlled the process by optimizing the superposition states belonging to S_2. The problem was first studied [6] using a simplified four-mode model for the pyrazine vibrational motion [9]. The optimization technique used showed the possibility of performing active phase control of $S_2 \leftrightarrow S_1$ interconversion, and that this control is directly related to the presence of overlapping resonances [10, 11] in the S_2 manifold. Subsequently [7, 8], the full 24-dimensional vibrational motion of pyrazine [12] was considered, and the dynamical problem solved using an efficient Löwdin-Feshbach QP-partitioning approach. Previous control results were fully confirmed and refined, proving the high controllability of $S_2 \leftrightarrow S_1$ internal conversion by actively exploiting the effect of quantum interferences which was shown to rely on the presence of overlapping resonances.

In Refs. [6, 8] coherent control was implemented for pyrazine that was already prepared in the excited S_2 state. The $S_0 \to S_2$ excitation process was not considered, assuming instead that the excited states in S_2 were already populated. Recently, we showed the possibility of performing effective coherent control in a simple IBr diatomic model, where we explicitly included the exciting laser in an approach that simultaneously considered excitation and decay to a continuum [13, 14]. In that case we introduced an optimization schemes different from the simple one used in Refs. [6, 8] and demonstrated the reliance of control on overlapping resonances. Below we considerably generalize this study to pyrazine, explicitly introducing the laser to excite the 24-dimensional $S_1 + S_2$ vibronic pyrazine model [7], and using the same control and optimization schemes as for IBr [13]. Significantly, we confirm the dependence of controllability on the properties of the S_2 resonances in pyrazine.

This paper is organized as follows. Section II reviews the theory explicitly accounting for the exciting laser in the weak field limit. Section III introduces the coherent control approach for the S_2 population, points out its connection with the properties of S_2 resonances, and provides additional details of the approach. Section IV provides computational results for control of pyrazine internal conversion. Section V provides a summary and conclusions.

II. $S_0 \to S_2$ EXCITATION AND $S_2 \leftrightarrow S_1$ INTERNAL CONVERSION

Below, $|\kappa\rangle$ denotes vibrational states belonging to the S_2 electronic state, with corresponding projection operator $Q = \sum_\kappa |\kappa\rangle\langle\kappa|$. Since the $|\kappa\rangle$ states are not eigenstates of the full Pyrazine Hamiltonian, the system evolves in time if it were prepared in these states. Hence, such states are termed resonances. The states $|\beta\rangle$ denote vibrational states belonging to the S_1 electronic state, with $P = \sum_\beta |\beta\rangle\langle\beta|$ being the associated projection operator. The full vibronic states, which are eigenstates of the full Pyrazine system, are denoted $|\gamma\rangle$, so that $P + Q = I = \sum_\gamma |\gamma\rangle\langle\gamma|$.

A. Time Evolution of the System Assumed Already Excited

In Refs. [6–8] $S_0 \to S_2$ laser excitation is assumed to allow preparation of a superposition of $|\kappa\rangle$ resonances:

$$|\Psi(0)\rangle = \sum_{\kappa'} c_{\kappa'} |\kappa'\rangle. \tag{1}$$

The dynamics of internal conversion was then described by an action of the propagator $U(t)$ on $|\Psi(0)\rangle$: $|\Psi(t)\rangle = U(t)|\Psi(0)\rangle$. Because $|\gamma\rangle$ are exact states of the system Hamiltonian, the spectral resolution of the evolution operator

$U(t) = \exp(-iHt/\hbar)$ is $U(t) = \sum_\gamma \exp(-iE_\gamma t/\hbar)|\gamma\rangle\langle\gamma|$. This gives

$$|\Psi(t)\rangle = \sum_{\kappa'} c_{\kappa'} \sum_\gamma \exp(-iE_\gamma t/\hbar)\langle\gamma|\kappa'\rangle|\gamma\rangle = \sum_\gamma a_\gamma \exp(-iE_\gamma t/\hbar)|\gamma\rangle, \tag{2}$$

where $a_\gamma \equiv \sum_{\kappa'} c_{\kappa'}\langle\gamma|\kappa'\rangle$.

The S_2 electronic state population P_{S_2} at time t is an observable defined by the projection operator Q onto the state $|\Psi(t)\rangle$:

$$P_{S_2}(t) = \langle\Psi(t)|Q|\Psi(t)\rangle = \sum_{\gamma',\gamma''} \tilde{a}^*_{\gamma'}(t)\, \tilde{a}_{\gamma''}(t) Q_{\gamma',\gamma''}, \tag{3}$$

where $\tilde{a}_\gamma(t) \equiv a_\gamma \exp(-iE_\gamma t/\hbar)$ and $Q_{\gamma',\gamma''} \equiv \langle\gamma'|Q|\gamma''\rangle$. Equation (3) can be rewritten in matrix form as:

$$P_{S_2}(t) = \mathbf{a}^\dagger \underline{\underline{\mathbf{e}}}^{iEt/\hbar} \mathbf{Q}\, \underline{\underline{\mathbf{e}}}^{-iEt/\hbar} \mathbf{a}, \tag{4}$$

where $\mathbf{a}$ is a vector with a_γ components, $\underline{\underline{\mathbf{e}}}^{\pm iEt/\hbar}$ are square diagonal matrices composed of $\exp(\pm iE_\gamma t/\hbar)$ values, and $\mathbf{Q}$ is a square matrix with $Q_{\gamma',\gamma''}$ matrix elements.

Since $Q = \sum_\kappa |\kappa\rangle\langle\kappa|$, the matrix elements $Q_{\gamma',\gamma''} = \langle\gamma'|Q|\gamma''\rangle = \sum_\kappa \langle\gamma'|\kappa\rangle\langle\gamma''|\kappa\rangle^*$. Introducing the matrix $\mathbf{R}$ with $R_{\gamma,\kappa} = \langle\gamma|\kappa\rangle$, then $Q_{\gamma',\gamma''} = \sum_\kappa R_{\gamma',\kappa} R^*_{\gamma'',k} = \sum_\kappa R_{\gamma',\kappa} R^\dagger_{\kappa,\gamma''} = [RR^\dagger]_{\gamma',\gamma''}$, giving

$$\mathbf{Q} = \mathbf{R}\mathbf{R}^\dagger. \tag{5}$$

In turn, according to Eq. (2), the vector $\mathbf{a}$ can be written as

$$\mathbf{a} = \mathbf{R}\mathbf{c}, \tag{6}$$

where $\mathbf{c}$ is a vector composed of $c_{\kappa'}$ coefficients. Inserting Eqs. (5) and (6) into Eq. (4) gives:

$$\begin{aligned} P_{S_2}(t) &= \mathbf{c}^\dagger\mathbf{R}^\dagger \underline{\underline{\mathbf{e}}}^{iEt/\hbar} \mathbf{R}\mathbf{R}^\dagger \underline{\underline{\mathbf{e}}}^{-iEt/\hbar} \mathbf{R}\mathbf{c} \equiv \mathbf{c}^\dagger \mathbf{M}^{c\dagger}(t)\mathbf{M}^c(t)\mathbf{c} \equiv \mathbf{c}^\dagger\mathbf{K}^c(t)\mathbf{c} \\ &= \sum_{\kappa',\kappa''} c^*_{\kappa'} c_{\kappa''} K^c_{\kappa',\kappa''}(t) = \sum_{\kappa'} |c_{\kappa'}|^2 K^c_{\kappa',\kappa'}(t) + \sum_{\kappa'\neq\kappa''} c^*_{\kappa'} c_{\kappa''} K^c_{\kappa',\kappa''}(t), \end{aligned} \tag{7}$$

where $\mathbf{M}^c(t)$ and $\mathbf{K}^c(t)$ matrices are defined as

$$\mathbf{M}^c(t) \equiv \mathbf{R}^\dagger \underline{\underline{\mathbf{e}}}^{-iEt/\hbar}\mathbf{R}, \qquad \mathbf{K}^c(t) \equiv \mathbf{M}^{c\dagger}(t)\mathbf{M}^c(t) = \mathbf{R}^\dagger \underline{\underline{\mathbf{e}}}^{iEt/\hbar}\mathbf{R}\mathbf{R}^\dagger \underline{\underline{\mathbf{e}}}^{-iEt/\hbar}\mathbf{R}. \tag{8}$$

The matrix elements of $\mathbf{M}^c(t)$ have the form

$$M^c_{\kappa,\kappa'}(t) = \sum_\gamma \langle\kappa|\gamma\rangle\langle\gamma|\kappa'\rangle \exp(-iE_\gamma t/\hbar) = \langle\kappa|U(t)|\kappa'\rangle, \tag{9}$$

being matrix elements of the $U(t)$ propagator operating between the resonances $|\kappa\rangle$ and $|\kappa'\rangle$. According to Eq. (9), $M^c_{\kappa,\kappa'}(t) \neq 0$ for $\kappa \neq \kappa'$, only if there is at least one state $|\gamma\rangle$ such that $\langle\kappa|\gamma\rangle \neq 0$ and $\langle\gamma|\kappa'\rangle \neq 0$. If so, then resonances $|\kappa\rangle$ and $|\kappa'\rangle$ are said to be overlapping. This resonance overlap property is crucial for $\mathbf{M}^c(t)$ nondiagonality which, in turn, provides $\mathbf{K}^c(t)$ nondiagonality, which allows efficient phase control of $P_{S_2}(t)$ in Eq. (7) by means of phases $\varphi_{\kappa'}$

of complex coefficients $c_{\kappa'} = |c_{\kappa'}| \exp(i\varphi_{\kappa'})$ [6, 8]. Such phase control is termed active control, in contrast to passive control, which is control via the $|c_{\kappa'}|$ amplitudes only.

In the case of pyrazine, which has 24 vibrational degrees of freedom, there is a large number of $|\gamma\rangle$ states [7, 12]. To make the computations feasible, instead of exact states, a set of approximate coarse-grained states is used to compute the time evolution. Specifically, the energy axis is divided into small bins I_α, of size Δ_α, center energy E_α and density of states ρ_α. The projector onto the coarse-grained state $|\alpha\rangle$ is then defined as:

$$|\alpha\rangle\langle\alpha| = (1/(\rho_\alpha\Delta_\alpha)) \sum_{\gamma\in I_\alpha} |\gamma\rangle\langle\gamma|, \quad \text{hence} \quad \sqrt{\rho_\alpha\Delta_\alpha}|\alpha\rangle\langle\alpha|\sqrt{\rho_\alpha\Delta_\alpha} = \sum_{\gamma\in I_\alpha} |\gamma\rangle\langle\gamma|.$$

Thus, the coarse-grained state $|\alpha\rangle$ effectively replaces all the $|\gamma\rangle$ states in the bin I_α. Numerically, the weighted states $|\overline{\alpha}\rangle \equiv \sqrt{\rho_\alpha\Delta_\alpha}|\alpha\rangle$ and their overlaps with resonances $|\kappa\rangle$ are available through our iterative solution method for pyrazine, based on QP-partitioning algorithm (described in detail in Ref. [7]), giving

$$|\overline{\alpha}\rangle\langle\overline{\alpha}| = \sum_{\gamma\in I_\alpha} |\gamma\rangle\langle\gamma|. \tag{10}$$

All the $|\gamma\rangle$ states belonging to the same bin I_α are treated as one effective state $|\alpha\rangle$; so that

$$\begin{aligned} M^c_{\kappa,\kappa'}(t) &= \sum_\gamma \langle\kappa|\gamma\rangle\langle\gamma|\kappa'\rangle \exp(-iE_\gamma t/\hbar) = \sum_\alpha \sum_{\gamma\in I_\alpha} \langle\kappa|\gamma\rangle\langle\gamma|\kappa'\rangle \exp(-iE_\gamma t/\hbar) \\ &\approx \sum_\alpha \langle\kappa|\alpha\rangle\langle\alpha|\kappa'\rangle\rho_\alpha\Delta_\alpha \cdot \frac{1}{\Delta_\alpha} \sum_{\gamma\in I_\alpha} \frac{1}{\rho_\alpha} \exp(-iE_\gamma t/\hbar). \end{aligned} \tag{11}$$

The remaining inner sum over $\gamma \in I_\alpha$ in Eq. (11) is approximated by a corresponding integral:

$$\begin{aligned} \frac{1}{\Delta_\alpha} \sum_{\gamma\in I_\alpha} \frac{1}{\rho_\alpha} \exp(-iE_\gamma t/\hbar) &\approx \frac{1}{\Delta_\alpha} \int_{E_\alpha-\Delta_\alpha/2}^{E_\alpha+\Delta_\alpha/2} dE_\gamma \exp(-iE_\gamma t/\hbar) \\ &= \exp(-iE_\alpha t/\hbar) \frac{\sin(\Delta_\alpha t/(2\hbar))}{\Delta_\alpha t/(2\hbar)} \equiv \tau_\alpha(t), \end{aligned} \tag{12}$$

giving the final coarse-grained expression for $M^c_{\kappa,\kappa'}(t)$:

$$M^c_{\kappa,\kappa'}(t) \approx \sum_\alpha \langle\kappa|\overline{\alpha}\rangle\langle\overline{\alpha}|\kappa'\rangle\tau_\alpha(t) = \langle\kappa| \left[\sum_\alpha \tau_\alpha(t)|\overline{\alpha}\rangle\langle\overline{\alpha}|\right] |\kappa'\rangle. \tag{13}$$

The quantity in the square brackets is the coarse-grained approximation to the $U(t)$ propagator, and the sum is over all available $|\overline{\alpha}\rangle$ states. Equation (13) is accurate for the evolution times which are not too large, i.e., when $|\tau_\alpha(t)| = |\sin(\Delta_\alpha t/(2\hbar))/(\Delta_\alpha t/(2\hbar))| \approx 1$, implying that $|t| \ll 2\hbar/\Delta_\alpha$. The resonance overlap phenomenon and the need for nonzero coarse-grained off-diagonal $M^c_{\kappa,\kappa'}(t)$ discussed above remains the same, except that the $|\gamma\rangle$ states are replaced by $|\overline{\alpha}\rangle$ states.

B. Time Evolution Due to Laser Excitation

Consider now the result of single photon excitation from the ground electronic state S_0, which produces the excited time-dependent wavepacket, as a superposition of $|\gamma\rangle$ states (here the subscript p denotes pulse):

$$|\Psi_p(t)\rangle = \sum_{\gamma} b_\gamma(t)\exp(-iE_\gamma t/\hbar)|\gamma\rangle, \tag{14}$$

where $b_\gamma(t)$ coefficients are, in general, time-dependent.

The S_2 electronic state population at time t is given by:

$$P_{S_2}(t) = \langle\Psi_p(t)|Q|\Psi_p(t)\rangle = \sum_{\gamma',\gamma''} \tilde{b}^*_{\gamma'}(t)\,\tilde{b}_{\gamma''}(t)Q_{\gamma',\gamma''}, \tag{15}$$

where $\tilde{b}_\gamma(t) \equiv b_\gamma(t)\exp(-iE_\gamma t/\hbar)$. Equation (15) can be written in matrix form as

$$P_{S_2}(t) = \mathbf{b}^\dagger(t)\underline{\underline{\mathbf{e}}}^{iEt/\hbar}\mathbf{Q}\,\underline{\underline{\mathbf{e}}}^{-iEt/\hbar}\mathbf{b}(t), \tag{16}$$

where $\mathbf{b}(t)$ is a vector composed of $b_\gamma(t)$ components.

If the exciting laser pulse is weak, first-order time-dependent perturbation theory is applicable, and the $b_\gamma(t)$ expansion coefficients in Eq. (14) can be written as

$$b_\gamma(t) = (i/\hbar)\langle\gamma|\mu|g\rangle\varepsilon_p(\omega_{\gamma,g},t), \tag{17}$$

where μ is the dipole operator, $|g\rangle$ is the ground vibrational state on S_0, $\omega_{\gamma,g} \equiv (E_\gamma - E_g)/\hbar$, and $\varepsilon_p(\omega_{\gamma,g},t)$ is the finite-time Fourier transform of the $\varepsilon_p(t)$:

$$\varepsilon_p(\omega_{\gamma,g},t) \equiv \int_{-\infty}^{t} dt'\varepsilon_p(t')\exp(i\omega_{\gamma,g}t'). \tag{18}$$

Eq. (17) can be written in matrix-vector form as

$$\mathbf{b}(t) = \underline{\underline{\mu}}\,\underline{\varepsilon}(t), \tag{19}$$

where $\underline{\underline{\mu}}$ is a square diagonal matrix composed of $(i/\hbar)\langle\gamma|\mu|g\rangle$ values, and $\underline{\varepsilon}(t)$ is a vector composed of $\varepsilon_p(\omega_{\gamma,g},t)$ components.

Inserting Eqs. (5) and (19) into Eq. (16) gives, for the $P_{S_2}(t)$ population,

$$\begin{aligned} P_{S_2}(t) &= \underline{\varepsilon}^\dagger(t)\underline{\underline{\mu}}^\dagger\underline{\underline{\mathbf{e}}}^{iEt/\hbar}\mathbf{R}\mathbf{R}^\dagger\underline{\underline{\mathbf{e}}}^{-iEt/\hbar}\underline{\underline{\mu}}\,\underline{\varepsilon}(t) \equiv \underline{\varepsilon}^\dagger(t)\mathbf{M}^{\varepsilon\dagger}(t)\mathbf{M}^{\varepsilon}(t)\underline{\varepsilon}(t) \equiv \underline{\varepsilon}^\dagger(t)\mathbf{K}^{\varepsilon}(t)\underline{\varepsilon}(t) \\ &= \sum_{\gamma'}|\varepsilon_p(\omega_{\gamma',g},t)|^2 K^{\varepsilon}_{\gamma',\gamma'}(t) + \sum_{\gamma'\neq\gamma''}\varepsilon^*_p(\omega_{\gamma',g},t)\varepsilon_p(\omega_{\gamma'',g},t)K^{\varepsilon}_{\gamma',\gamma''}(t), \end{aligned} \tag{20}$$

where $\mathbf{M}^{\varepsilon}(t)$ and $\mathbf{K}^{\varepsilon}(t)$ matrices are defined as

$$\mathbf{M}^{\varepsilon}(t) \equiv \mathbf{R}^\dagger\underline{\underline{\mathbf{e}}}^{-iEt/\hbar}\underline{\underline{\mu}}, \qquad \mathbf{K}^{\varepsilon}(t) \equiv \mathbf{M}^{\varepsilon\dagger}(t)\mathbf{M}^{\varepsilon}(t). \tag{21}$$

Since $\underline{\underline{\mu}}$ and $\underline{\underline{\mathbf{e}}}^{\pm iEt/\hbar}$ are diagonal, the only source of nondiagonality in Eqs. (20) and (21) for $\mathbf{K}^{\varepsilon}(t)$ is $\mathbf{Q} = \mathbf{R}\mathbf{R}^{\dagger}$. Thus, phase control via the phases $\phi_{\gamma}(t)$ of complex $\varepsilon_p(\omega_{\gamma,g}, t) = |\varepsilon_p(\omega_{\gamma,g}, t)| \exp(i\phi_{\gamma}(t))$, depends solely on properties of $\mathbf{Q}$.

A few comments are in order. First, $\mathbf{R}$ is a rectangular matrix, with each κ^{th} column composed of overlaps $R_{\gamma,\kappa} = \langle\gamma|\kappa\rangle$ of the resonance $|\kappa\rangle$ with all $|\gamma\rangle$ states. On the one hand, each resonance, being broadened in energy, has more than one nonzero $\langle\gamma|\kappa\rangle$ term in its κ_{th} own column. On the other hand, if resonances $|\kappa\rangle$ and $|\kappa'\rangle$ overlap, then they have at least one common $|\gamma\rangle$ such that, for this $|\gamma\rangle$, both $R_{\gamma,\kappa} \neq 0$ and $R_{\gamma,\kappa'} \neq 0$ simultaneously.

Second, all nonzero $\langle\gamma|\kappa\rangle$ components of each column in the $\mathbf{R}$ matrix that are related to one particular resonance $|\kappa\rangle$ form a square block centered along the main diagonal in the resulting $\mathbf{Q} = \mathbf{R}\mathbf{R}^{\dagger}$ matrix, filled by terms $Q_{\gamma',\gamma''} = \langle\gamma'|\kappa\rangle\langle\kappa|\gamma''\rangle$. Thus, $\mathbf{Q}$ displays block-diagonal structure. Since each block dimensionality is larger than one due to resonance energy broadening, nondiagonal matrix elements in these blocks are generally nonzero, contributing to $\mathbf{K}^{\varepsilon}(t)$ nondiagonality, and thereby providing $P_{S_2}(t)$ phase control *associated with the energy broadening of each particular resonance*. This kind of control will be discussed below. Furthermore, if resonances $|\kappa\rangle$ and $|\kappa'\rangle$ overlap, then the corresponding blocks overlap, so that the $\mathbf{Q}$ matrix acquires a non-block-diagonal structure. In this case $Q_{\gamma',\gamma''}$ matrix elements belonging to two blocks simultaneously are a sum of terms borrowed from each block (produced by its corresponding resonance): $Q_{\gamma',\gamma''} = \langle\gamma'|\kappa\rangle\langle\kappa|\gamma''\rangle + \langle\gamma'|\kappa'\rangle\langle\kappa'|\gamma''\rangle$. Similarly, in the case of overlap of N blocks, the sum contains N terms: $Q_{\gamma',\gamma''} = \sum_{\kappa=\kappa_1}^{\kappa_N} \langle\gamma'|\kappa\rangle\langle\kappa|\gamma''\rangle$. As will be discussed below, *the resonance overlap effect greatly increases the overall phase controllability in comparison with a pure resonance energy broadening effect.*

The nondiagonality in this section (see above), is very different from that discussed in Sect. II A. Specifically, in Eq. (7), for the case when the system is already assumed to be excited, control is performed by means of the $c_{\kappa'}$ coeeficients, so that $\mathbf{a} = \mathbf{R}\,\mathbf{c}$, giving $\mathbf{K}^{c}(t) = \mathbf{R}^{\dagger}\underline{\underline{\mathbf{e}}}^{iEt/\hbar}\mathbf{R}\mathbf{R}^{\dagger}\underline{\underline{\mathbf{e}}}^{-iEt/\hbar}\mathbf{R}$ [Eq. (8)]. This greatly simplifies the $\mathbf{K}^{c}(t)$ nondiagonality dependence, effectively removing the resonance broadening effect and leaving only resonance overlap as the crucial effect that provides nondiagonality, *i.e.*, phase control. By contrast, in this section, $\mathbf{K}^{\varepsilon}(t) = \underline{\underline{\mu}}^{\dagger}\underline{\underline{\mathbf{e}}}^{iEt/\hbar}\mathbf{R}\mathbf{R}^{\dagger}\underline{\underline{\mathbf{e}}}^{-iEt/\hbar}\underline{\underline{\mu}}$ [Eq. (21)] and nondiagonality is provided only by the $\mathbf{Q} = \mathbf{R}\mathbf{R}^{\dagger}$ matrix itself, whose nondiagonality, responsible for phase control, depends on *both* resonance broadening and resonance overlap effects.

It can be noted that $\mathbf{M}^{\varepsilon}(t)\underline{\varepsilon}(t)$ in Eq. (20) is a vector composed of components

$$\langle\kappa|\Psi_p(t)\rangle = \sum_{\gamma} \varepsilon_p(\omega_{\gamma,g}, t) M^{\varepsilon}_{\kappa,\gamma}(t) = \sum_{\gamma} \varepsilon_p(\omega_{\gamma,g}, t) \left[\langle\kappa|\gamma\rangle \exp(-iE_{\gamma}t/\hbar)\frac{i}{\hbar}\langle\gamma|\mu|g\rangle\right]. \tag{22}$$

In the case of pyrazine, transition dipole matrix elements for the $S_0 \to S_1$ excitation are an order of magnitude smaller than for the $S_0 \to S_2$ excitation [6–8, 15], thus allowing the following "doorway" approximation:

$$\langle\gamma|\mu|g\rangle = \langle\gamma|(P+Q)\mu|g\rangle = \sum_{\beta}\langle\gamma|\beta\rangle\langle\beta|\mu|g\rangle + \sum_{\kappa}\langle\gamma|\kappa\rangle\langle\kappa|\mu|g\rangle \approx \sum_{\kappa}\langle\gamma|\kappa\rangle\langle\kappa|\mu|g\rangle. \tag{23}$$

Equation (23) indicates that the excitation to a full vibronic state $|\gamma\rangle$ takes place by means of a preliminary intermediate transition to a manifold of $|\kappa\rangle$ resonances. Inserting Eq. (23) into Eq. (22) gives

$$\langle\kappa|\Psi_p(t)\rangle = \sum_\gamma \varepsilon_p(\omega_{\gamma,g},t)\left[\langle\kappa|\gamma\rangle\exp(-iE_\gamma t/\hbar)\frac{i}{\hbar}\sum_{\kappa'}\langle\gamma|\kappa'\rangle\langle\kappa'|\mu|g\rangle\right], \tag{24}$$

which can be rewritten as

$$\langle\kappa|\Psi_p(t)\rangle = \sum_{\kappa'}\frac{i}{\hbar}\langle\kappa'|\mu|g\rangle\left[\sum_\gamma \varepsilon_p(\omega_{\gamma,g},t)\langle\kappa|\gamma\rangle\langle\gamma|\kappa'\rangle\exp(-iE_\gamma t/\hbar)\right]. \tag{25}$$

In order to make the computations below feasible, we introduce here a coarse-graining procedure for the quantity in square brackets in Eq. (25). This procedure is similar to the one made in Ref. [7], taking into account Eqs. (11) and (12). Namely, $\sum_\gamma$ is written as $\sum_\alpha\sum_{\gamma\in I_\alpha}$:

$$\begin{aligned}\sum_\alpha\sum_{\gamma\in I_\alpha}\varepsilon_p(\omega_{\gamma,g},t)\langle\kappa|\gamma\rangle\langle\gamma|\kappa'\rangle\exp(-iE_\gamma t/\hbar) &\approx \sum_\alpha \varepsilon_p(\omega_{\alpha,g},t)\langle\kappa|\alpha\rangle\langle\alpha|\kappa'\rangle\rho_\alpha\Delta_\alpha\cdot\frac{1}{\Delta_\alpha}\sum_{\gamma\in I_\alpha}\frac{1}{\rho_\alpha}\exp(-iE_\gamma t/\hbar)\\ &\approx \sum_\alpha \varepsilon_p(\omega_{\alpha,g},t)\langle\kappa|\overline{\alpha}\rangle\langle\overline{\alpha}|\kappa'\rangle\tau_\alpha(t),\end{aligned} \tag{26}$$

where $\omega_{\alpha,g}\equiv(E_\alpha-E_g)/\hbar$. Inserting Eq. (26) into Eq. (25) gives:

$$\langle\kappa|\Psi_p(t)\rangle \approx \sum_\alpha \varepsilon_p(\omega_{\alpha,g},t)\left[\langle\kappa|\overline{\alpha}\rangle\,\tau_\alpha(t)\,\frac{i}{\hbar}\sum_{\kappa'}\langle\overline{\alpha}|\kappa'\rangle\langle\kappa'|\mu|g\rangle\right] \equiv \sum_\alpha \varepsilon_p(\omega_{\alpha,g},t)M^{\varepsilon,\alpha}_{\kappa,\alpha}(t). \tag{27}$$

Below, a superscript α indicates the coarse-grained nature of the corresponding values. Here, the quantity

$$M^{\varepsilon,\alpha}_{\kappa,\alpha}(t) \equiv \langle\kappa|\overline{\alpha}\rangle\,\tau_\alpha(t)\,\frac{i}{\hbar}\sum_{\kappa'}\langle\overline{\alpha}|\kappa'\rangle\langle\kappa'|\mu|g\rangle \equiv \langle\kappa|\,[\,\tau_\alpha(t)|\overline{\alpha}\rangle\langle\overline{\alpha}|\,]\left[\sum_{\kappa'}\frac{i}{\hbar}\langle\kappa'|\mu|g\rangle|\kappa'\rangle\right] \tag{28}$$

is a coarse-grained version of $M^{\varepsilon}_{\kappa,\gamma}(t)$ [Eq. (22)] and depends only on the material system properties. If one defines

$$\mu^\alpha_\alpha \equiv \frac{i}{\hbar}\sum_{\kappa'}\langle\overline{\alpha}|\kappa'\rangle\langle\kappa'|\mu|g\rangle = \frac{i}{\hbar}\langle\overline{\alpha}|\mu|g\rangle, \qquad R^\alpha_{\alpha,\kappa}\equiv\langle\overline{\alpha}|\kappa\rangle, \tag{29}$$

then

$$\mathbf{M}^{\varepsilon,\alpha}(t) = \mathbf{R}^{\alpha\dagger}\,\underline{\underline{\tau}}^\alpha(t)\,\underline{\underline{\mu}}^\alpha, \qquad \mathbf{K}^{\varepsilon,\alpha}(t) = \mathbf{M}^{\varepsilon,\alpha\dagger}(t)\mathbf{M}^{\varepsilon,\alpha}(t), \tag{30}$$

where $\underline{\underline{\tau}}^\alpha(t)$ is a square diagonal matrix composed of $\tau_\alpha(t)$ values, and $\underline{\underline{\mu}}^\alpha$ is a square diagonal matrix composed of $(i/\hbar)\langle\overline{\alpha}|\mu|g\rangle$ values. Then the $P_{S_2}(t)$ population in terms of coarse-grained values becomes

$$\begin{aligned}P_{S_2}(t) &= \underline{\varepsilon}^{\alpha\dagger}(t)\mathbf{M}^{\varepsilon,\alpha\dagger}(t)\mathbf{M}^{\varepsilon,\alpha}(t)\,\underline{\varepsilon}^\alpha(t) \equiv \underline{\varepsilon}^{\alpha\dagger}(t)\mathbf{K}^{\varepsilon,\alpha}(t)\,\underline{\varepsilon}^\alpha(t)\\ &= \sum_{\alpha'}|\varepsilon_p(\omega_{\alpha',g},t)|^2K^{\varepsilon,\alpha}_{\alpha',\alpha'}(t) + \sum_{\alpha'\neq\alpha''}\varepsilon_p^*(\omega_{\alpha',g},t)\varepsilon_p(\omega_{\alpha'',g},t)K^{\varepsilon,\alpha}_{\alpha',\alpha''}(t),\end{aligned} \tag{31}$$

where $\underline{\varepsilon}^\alpha(t)$ is a vector composed of $\varepsilon_p(\omega_{\alpha,g},t)$ components.

The quantities $\underline{\underline{\mu}}^\alpha$ and $\underline{\underline{\tau}}^\alpha(t)$ are diagonal matrices, so the only origin of nondiagonality in Eq. (30) for $\mathbf{K}^{\varepsilon,\alpha}(t)$ and Eq. (31) is via the $\mathbf{Q}^\alpha = \mathbf{R}^\alpha\mathbf{R}^{\alpha\dagger}$ matrix, composed of $Q^\alpha_{\alpha',\alpha''} = \langle\overline{\alpha}'|Q|\overline{\alpha}''\rangle$ matrix elements. Hence, all the $P_{S_2}(t)$ phase control considerations from above remain the same, except that $|\gamma\rangle$ states are replaced by $|\overline{\alpha}\rangle$ states. Namely, *phase control is driven both by resonance energy broadening and resonance overlap. The resonance overlap effect, providing a non-block-diagonal structure of* $\mathbf{Q}^\alpha$ *and* $\mathbf{K}^{\varepsilon,\alpha}(t)$, *strongly enhances the effect of resonance broadening.*

III. COHERENT CONTROL OF PYRAZINE INTERNAL CONVERSION

Section II B above describes resonance broadening and resonance overlap, two effects related to $\mathbf{Q}$ ($\mathbf{Q}^{\alpha}$) and $\mathbf{K}^{\varepsilon}(t)$ ($\mathbf{K}^{\varepsilon,\alpha}(t)$) nondiagonality. Here, a control scheme based on resonance broadening is discussed in Sect. III A. Section III B discusses a control scheme relying on presence of resonance overlap.

A. Control Associated with Single Resonance

In the case of pure resonance broadening without resonance overlap, one particular resonance $|\kappa\rangle$ has nonzero $R_{\gamma,\kappa} = \langle\gamma|\kappa\rangle$ terms for some specific set $\{\gamma\}_{\kappa}$ of $|\gamma\rangle$ states. This results in the simplified expressions for $\mathbf{K}^{\varepsilon}(t)$ matrix elements for this $\{\gamma\}_{\kappa}$ set, with the summation over κ reduced to a single term

$$K^{\varepsilon}_{\gamma',\gamma'}(t) = |M^{\varepsilon}_{\kappa,\gamma'}(t)|^2, \qquad K^{\varepsilon}_{\gamma',\gamma''}(t) = M^{\varepsilon *}_{\kappa,\gamma'}(t) M^{\varepsilon}_{\kappa,\gamma''}(t) \tag{32}$$

for the diagonal and nondiagonal matrix elements, respectively.

The probability $P_{S_2}(t)$ [Eq. (20)] is a quadratic form of complex time-dependent variables $\varepsilon_p(\omega_{\gamma,g},t)$. When the pulse is already over (at $t = T_{over}$), these values become infinite-time Fourier transforms of this laser pulse at different frequencies, $\varepsilon_p(\omega_{\gamma,g})$; they are no longer time-dependent for $t \geq T_{over}$. Here we use the so-called absolute control scheme for $P_{S_2}(t)$ optimization, with the $\mathbf{K}^{\varepsilon}(t)$ matrix given in Eq. (32). Namely, $P_{S_2}(t)$ is optimized at a desired optimization time $t = T$, while keeping the total energy of the pulse at $2\pi E_0$:

$$\sum_{\{\gamma\}_{\kappa}} |\varepsilon_p(\omega_{\gamma,g})|^2 = \underline{\varepsilon}^{\dagger}\underline{\varepsilon} = 2\pi E_0. \tag{33}$$

This is done by introducing the corresponding Lagrange multiplier λ^A (superscript A denotes absolute) with the corresponding optimization function at time T defined as:

$$P^{\lambda;A}_{S_2}(T,\underline{\varepsilon}) = \underline{\varepsilon}^{\dagger}\mathbf{K}^{\varepsilon}(T)\underline{\varepsilon} - \lambda^A(\underline{\varepsilon}^{\dagger}\underline{\varepsilon} - 2\pi E_0). \tag{34}$$

We then search for $P^{\lambda;A}_{S_2}(T,\underline{\varepsilon})$ extrema with respect to $\underline{\varepsilon}$:

$$\begin{cases} \dfrac{\partial P^{\lambda;A}_{S_2}(T,\underline{\varepsilon})}{\partial\,\mathrm{Re}\,[\varepsilon_p(\omega_{\gamma,g})]} = 0, \\ \dfrac{\partial P^{\lambda;A}_{S_2}(T,\underline{\varepsilon})}{\partial\,\mathrm{Im}\,[\varepsilon_p(\omega_{\gamma,g})]} = 0, \qquad \gamma = 1,\ldots,N_{\{\gamma\}_{\kappa}}, \end{cases} \tag{35}$$

where $N_{\{\gamma\}_{\kappa}}$ is the number of $|\gamma\rangle$ states in the set $\{\gamma\}_{\kappa}$. Conditions in Eq. (35), applied to Eq. (34), lead directly to an eigenvalue problem

$$\mathbf{K}^{\varepsilon}(T)\underline{\varepsilon} = \lambda^A\underline{\varepsilon}. \tag{36}$$

which provides a set of eigenvalues λ^A and corresponding eigenvectors $\underline{\varepsilon}$ with a unit norm ($\underline{\varepsilon}^{\dagger}\underline{\varepsilon} = 1$). Multiplication of these $\underline{\varepsilon}$ eigenvectors by $\sqrt{2\pi E_0}$ provides the required optimized solutions.

The $\mathbf{K}^{\varepsilon}(t)$ matrix is such that all but one of its $N_{\{\gamma\}_\kappa}$ eigenvalues are equal exactly to 0, while its last eigenvalue is equal to the sum of its diagonal elements:

$$\lambda_n^A = 0, \qquad n = 1, \ldots, N_{\{\gamma\}_\kappa} - 1; \qquad \lambda^A_{N_{\{\gamma\}_\kappa}} = \sum_{\{\gamma\}_\kappa} K^{\varepsilon}_{\gamma,\gamma}(t) = \sum_{\{\gamma\}_\kappa} |M^{\varepsilon}_{\kappa,\gamma}(t)|^2. \tag{37}$$

This is an analytical property of the $\mathbf{K}^{\varepsilon}(t)$ matrix in Eq. (32), so that a numerical solution of the eigenproblem in [Eq. (36)] is not required. Specifically, *for any time T, $P_{S_2}(T)$ can be set to zero, using the eigenvector corresponding to zero eigenvalue.* In terms of the coarse-grained $|\overline{\alpha}\rangle$ states, the results are the same with the $\{\gamma\}_\kappa$ set replaced by $\{\overline{\alpha}\}_\kappa$.

Given the simplistic nature of this solution, numerical results are neither necessary nor are they provided below. Note, however, that this type of control is possible only if the system displays isolated resonances. This can be the case in small molecules; large molecules such as pyrazine, however, display overlapping resonances throughout the spectrum, with highly unlikely regions of isolated resonance. Such systems can be controlled via an alternate mechanism, discussed below.

B. Control Associated with Overlapping Resonances

Here we consider a second different control scheme, termed relative control. Namely, we optimize the *ratio* of $P_{S_2}(t)$ populations at times T_2 and T_1, where $T_2 > T_1 \geq T_{over}$:

$$\lambda^R = \frac{P_{S_2}(T_2)}{P_{S_2}(T_1)} \to \max, \min \tag{38}$$

(where superscript R denotes relative). One can optimize the value of $P_{S_2}(T_2)$, keeping the value of $P_{S_2}(T_1)$ constant [16] and equal to some predefined value P_0. Here fixed $P_{S_2}(T_1) = P_0$ assures that enhanced (or diminished) P_{S_2} at the target final time T_2 does not simply result from a stronger (or weaker) field that simply achieves control by affecting the amount of S_2 excited. To do so, we consider the optimization function

$$P^{\lambda;R}_{S_2}(T_2, T_1, \underline{\varepsilon}) = \underline{\varepsilon}^{\dagger}\mathbf{K}^{\varepsilon}(T_2)\underline{\varepsilon} - \lambda^R(\underline{\varepsilon}^{\dagger}\mathbf{K}^{\varepsilon}(T_1)\underline{\varepsilon} - P_0), \tag{39}$$

where λ^R is a yet unknown Lagrange multiplier. We then find $P^{\lambda;R}_{S_2}(T_2, T_1, \underline{\varepsilon})$ extrema with respect to $\underline{\varepsilon}$ leading directly to a generalized eigenvalue problem:

$$\mathbf{K}^{\varepsilon}(T_2)\underline{\varepsilon} = \lambda^R \mathbf{K}^{\varepsilon}(T_1)\underline{\varepsilon}. \tag{40}$$

Multiplying Eq. (40) by $\underline{\varepsilon}^{\dagger}$ from the left gives

$$\underline{\varepsilon}^{\dagger}\mathbf{K}^{\varepsilon}(T_2)\underline{\varepsilon} = \lambda^R \underline{\varepsilon}^{\dagger}\mathbf{K}^{\varepsilon}(T_1)\underline{\varepsilon}. \tag{41}$$

The λ^R is real and positive because $\underline{\varepsilon}^\dagger \mathbf{K}^\varepsilon(T_2)\underline{\varepsilon} = P_{S_2}(T_2)$ and $\underline{\varepsilon}^\dagger \mathbf{K}^\varepsilon(T_1)\underline{\varepsilon} = P_{S_2}(T_1)$ are real positive values. Dividing Eq. (41) by $\underline{\varepsilon}^\dagger \mathbf{K}^\varepsilon(T_1)\underline{\varepsilon}$, yields $\lambda^R = P_{S_2}(T_2)/P_{S_2}(T_1)$, i.e., λ^R is the optimized ratio of the populations of interest [Eq. (38)].

The $\mathbf{K}^\varepsilon(t)$ matrix determinant is generally nonzero at every time t, so that $\mathbf{K}^\varepsilon(t)$ always has an inverse $[\mathbf{K}^\varepsilon(t)]^{-1}$. This allows transformation of the generalized eigenvalue problem in Eq. (40) into an ordinary eigenvalue problem. To do this, we multiply the left and right sides of Eq. (40) by $[\mathbf{K}^\varepsilon(T_1)]^{-1}$ from the left:

$$\mathbf{R}^\varepsilon(T_2,T_1)\underline{\varepsilon} = \lambda^R \underline{\varepsilon}, \tag{42}$$

$$\mathbf{R}^\varepsilon(T_2,T_1) \equiv [\mathbf{K}^\varepsilon(T_1)]^{-1}\mathbf{K}^\varepsilon(T_2). \tag{43}$$

The solution to the eigenproblem in Eq. (42) for times $T_2 > T_1 \geq T_{over}$ is dependent only on the properties of the material system. Moreover, this solution is the best possible in the weak field case, i.e., it is optimal [17]. Specifically, the maximal and minimal eigenvalues λ^R provide the entire achievable range of $P_{S_2}(T_2)/P_{S_2}(T_1)$ for a given T_2 and T_1, obtained using the corresponding eigenvectors $\underline{\varepsilon}$.

In terms of coarse-grained states $|\overline{\alpha}\rangle$, $\underline{\varepsilon}$ is replaced by $\underline{\varepsilon}^\alpha$, and $\mathbf{K}^\varepsilon(t)$ is replaced by $\mathbf{K}^{\varepsilon,\alpha}(t)$, giving the following coarse-grained version of the optimization problem:

$$\mathbf{R}^{\varepsilon,\alpha}(T_2,T_1)\underline{\varepsilon}^\alpha = \lambda^{R,\alpha}\underline{\varepsilon}^\alpha, \tag{44}$$

$$\mathbf{R}^{\varepsilon,\alpha}(T_2,T_1) \equiv [\mathbf{K}^{\varepsilon,\alpha}(T_1)]^{-1}\mathbf{K}^{\varepsilon,\alpha}(T_2). \tag{45}$$

In addressing this problem computationally, we encountered numerical instability in Eq. (44) if the number of $|\overline{\alpha}\rangle$ states is relatively large (150–180). Namely, the condition number of $\mathbf{K}^{\varepsilon,\alpha}(t)$ tends to become very large, resulting in an ill-conditioned matrix, preventing accurate numerical construction of $\mathbf{R}^{\varepsilon,\alpha}(T_2,T_1)$ [Eq. (45)] and its subsequent diagonalization. To overcome this problem, we partitioned the energy axis into a limited number of N_A bins in Eq. (27), as discussed in the Appendix, giving further broadened $|\mathbf{A}\rangle$ states.

Using these further broadened $|\mathbf{A}\rangle$ states allows us to reformulate the eigenproblem in Eq. (44) as

$$\mathbf{R}^{\varepsilon,\mathbf{A}}(T_2,T_1)\underline{\varepsilon}^\mathbf{A} = \lambda^{R,\mathbf{A}}\underline{\varepsilon}^\mathbf{A}, \tag{46}$$

$$\mathbf{R}^{\varepsilon,\mathbf{A}}(T_2,T_1) \equiv [\mathbf{K}^{\varepsilon,\mathbf{A}}(T_1)]^{-1}\mathbf{K}^{\varepsilon,\mathbf{A}}(T_2), \tag{47}$$

where the states $|\bar{\alpha}\rangle$ in Eqs. (44) and (45) are replaced by the further broadened states $|\mathbf{A}\rangle$, as described in the Appendix.

C. Numerical Correlation between Controllability and Resonance Overlap

In general, effects of resonance energy broadening and resonance overlap are mixed together in the structure of the $\mathbf{Q}^\mathbf{A}$ and $\mathbf{K}^{\varepsilon,\mathbf{A}}(t)$ matrices. To quantitatively estimate the $\mathbf{K}^{\varepsilon,\mathbf{A}}(t)$ nondiagonality, providing phase control, we utilize the Hadamard measure:

$$H\left(\mathbf{K}^{\varepsilon,\mathbf{A}}(t)\right) = \det\left(\mathbf{K}^{\varepsilon,\mathbf{A}}(t)\right)/\det\left(\operatorname{diag}\left(\mathbf{K}^{\varepsilon,\mathbf{A}}(t)\right)\right), \tag{48}$$

where det denotes a determinant, and diag is the diagonal part of a matrix. Thus, $\det\left(\operatorname{diag}\left(\mathbf{K}^{\varepsilon,\mathbf{A}}(t)\right)\right) = \prod_{A=1}^{N_A} K^{\varepsilon,\mathbf{A}}_{A,A}(t)$. Since $\mathbf{K}^{\varepsilon,\mathbf{A}}(t)$ is a Hermitian positive-definite matrix, both $\det\left(\mathbf{K}^{\varepsilon,\mathbf{A}}(t)\right)$ and $\det\left(\operatorname{diag}\left(\mathbf{K}^{\varepsilon,\mathbf{A}}(t)\right)\right)$ are real and positive. Furthermore, $\det\left(\mathbf{K}^{\varepsilon,\mathbf{A}}(t)\right) \leq \det\left(\operatorname{diag}\left(\mathbf{K}^{\varepsilon,\mathbf{A}}(t)\right)\right)$, giving

$$0 < H\left(\mathbf{K}^{\varepsilon,\mathbf{A}}(t)\right) \leq 1, \tag{49}$$

where the equality applies if and only if $\mathbf{K}^{\varepsilon,\mathbf{A}}(t)$ is strictly diagonal.

The determinant of $\mathbf{R}^{\varepsilon,\mathbf{A}}(T_2, T_1)$ can be expressed as

$$\det\left(\mathbf{R}^{\varepsilon,\mathbf{A}}(T_2,T_1)\right) = \det\left[\left[\mathbf{K}^{\varepsilon,\mathbf{A}}(T_1)\right]^{-1}\mathbf{K}^{\varepsilon,\mathbf{A}}(T_2)\right] = \det\left(\mathbf{K}^{\varepsilon,\mathbf{A}}(T_2)\right)/\det\left(\mathbf{K}^{\varepsilon,\mathbf{A}}(T_1)\right). \tag{50}$$

Hadamard-like measures of non-diagonality for $\mathbf{R}^{\varepsilon,\mathbf{A}}(t)$ are introduced in a similar manner:

$$H_R\left(\mathbf{R}^{\varepsilon,\mathbf{A}}(T_2,T_1)\right) = \frac{\det\left(\mathbf{R}^{\varepsilon,\mathbf{A}}(T_2,T_1)\right)}{\det\left[\operatorname{diag}([\mathbf{K}^{\varepsilon,\mathbf{A}}(T_1)]^{-1})\ \operatorname{diag}(\mathbf{K}^{\varepsilon,\mathbf{A}}(T_2))\right]} = \frac{H\left(\mathbf{K}^{\varepsilon,\mathbf{A}}(T_2)\right)}{\det[\operatorname{diag}([\mathbf{K}^{\varepsilon,\mathbf{A}}(T_1)]^{-1})]\cdot\det(\mathbf{K}^{\varepsilon,\mathbf{A}}(T_1))}, \tag{51}$$

$$H_C\left(\mathbf{R}^{\varepsilon,\mathbf{A}}(T_2,T_1)\right) = \frac{\det(\mathbf{R}^{\varepsilon,\mathbf{A}}(T_2,T_1))}{\det(\operatorname{diag}(\mathbf{R}^{\varepsilon,\mathbf{A}}(T_2,T_1)))} = \frac{\det(\mathbf{K}^{\varepsilon,\mathbf{A}}(T_2))}{\det(\operatorname{diag}(\mathbf{R}^{\varepsilon,\mathbf{A}}(T_2,T_1)))\cdot\det(\mathbf{K}^{\varepsilon,\mathbf{A}}(T_1))}, \tag{52}$$

where Eq. (50) is used. The subscript R denotes real, and subscript C denotes complex. $H_R\left(\mathbf{R}^{\varepsilon,\mathbf{A}}(T_2,T_1)\right)$ is real because both its numerator and denominator are real.

In order to quantitatively estimate the extent of resonance overlap, we use the same overlap matrix as in Ref. [8], but include only the $|\overline{\alpha}\rangle$ states, which are populated by the exciting laser spanning the energy range $[E_L, E_H]$:

$$\Omega^{\alpha}_{\kappa,\kappa'} = \sum_{\alpha, E_\alpha\in[E_L,E_H]} |\langle\kappa|\overline{\alpha}\rangle|\cdot|\langle\overline{\alpha}|\kappa'\rangle|\,. \tag{53}$$

The Hadamard non-diagonality measure for the $\mathbf{\Omega}^{\alpha}$ matrix of size $N_Q \times N_Q$, composed of $\Omega^{\alpha}_{\kappa,\kappa'}$ values, is introduced as

$$H\left(\mathbf{\Omega}^{\alpha}\right) = \det\left(\mathbf{\Omega}^{\alpha}\right)/\det\left(\operatorname{diag}\left(\mathbf{\Omega}^{\alpha}\right)\right). \tag{54}$$

The numerator in Eq. (54) is shown numerically to be always real and positive, and the denominator is equal to $\prod_{\kappa=1}^{N_Q}\Omega^{\alpha}_{\kappa,\kappa}$, and thus also real and positive. The same inequality as in Eq. (49) is valid for $H\left(\mathbf{\Omega}^{\alpha}\right)$.

D. Implementation of the Shaped Laser as a Linear Combination of Gaussian Laser Pulses

The eigenvector $\underline{\varepsilon}^{\mathbf{A}}$ providing the desired optimized value $\lambda^{R,\mathbf{A}}$ after the pulse is over [Eq. (46)] is a finite discrete set of complex values of laser amplitudes $\varepsilon_p(\omega_{A,g})$, at different frequencies. These values can be reached in multiple ways. The approach used for the IBr model [13], is also used here: namely, to obtain the desired set of $\varepsilon_p(\omega_{A,g})$ values, $A = 1, \ldots, N_A$, it is sufficient to take the same number of linearly independent functions $\varepsilon_a(\omega)$, and expand the components of $\underline{\varepsilon}^{\mathbf{A}}$ in terms of $\varepsilon_a(\omega)$ at all $\omega_{A,g}$ frequencies with the (as yet unknown) time-independent complex coefficients d_a:

$$\varepsilon_p(\omega_{A,g}) = \sum_a d_a \varepsilon_a(\omega_{A,g}), \qquad a, A = 1, \ldots, N_A, \qquad t \geq T_{over}. \tag{55}$$

or, as a matrix equation:

$$\underline{\varepsilon}^{\mathbf{A}} = \mathbf{B}\,\mathbf{d}, \qquad B_{A,a} = \varepsilon_a(\omega_{A,g}), \qquad \mathbf{d} = (d_1, \ldots, d_{N_A})^T, \qquad t \geq T_{over}. \tag{56}$$

The set of $\varepsilon_a(\omega)$ functions is linearly independent, the $\mathbf{B}$ determinant is nonzero, and the unique nonzero vector $\mathbf{d}$ exists as a solution of Eq. (56), found as

$$\mathbf{d} = [\mathbf{B}]^{-1} \underline{\varepsilon}^{\mathbf{A}}. \tag{57}$$

The basis functions $\varepsilon_a(\omega)$ in frequency domain can be assumed to be *infinite-time* Fourier transforms of the corresponding basis functions $\varepsilon_a(t)$ in time domain (the latter are all vanishing when $t \geq T_{over}$). In turn, *finite-time* Fourier transforms of $\varepsilon_a(t)$ can be written as $\varepsilon_a(\omega, t)$, and at finite times Eq. (55) takes the form:

$$\varepsilon_p(\omega_{A,g}, t) = \sum_a d_a \varepsilon_a(\omega_{A,g}, t), \qquad a, A = 1, \ldots, N_A, \tag{58}$$

i.e.,

$$\underline{\varepsilon}^{\mathbf{A}}(t) = \mathbf{B}(t)\mathbf{d}, \qquad B_{A,a}(t) = \varepsilon_a(\omega_{A,g}, t), \qquad \mathbf{d} = (d_1, \ldots, d_{N_A})^T. \tag{59}$$

Using Eq. (59), $P_{S_2}(t)$, Eq. (75), can be expressed in terms of the $\mathbf{d}$ vector:

$$P_{S_2}(t) = \underline{\varepsilon}^{\mathbf{A}\dagger}(t)\mathbf{K}^{\varepsilon,\mathbf{A}}(t)\underline{\varepsilon}^{\mathbf{A}}(t) = \mathbf{d}^\dagger \mathbf{B}^\dagger(t)\mathbf{K}^{\varepsilon,\mathbf{A}}(t)\mathbf{B}(t)\mathbf{d}. \tag{60}$$

Thus, the $\mathbf{d}$ vector in Eq. (57) can be used for time propagation of $P_{S_2}(t)$ [Eq. (60)] at all times: before the laser is turned on, while the laser is on, and after the laser is off. Optimized populations always satisfy the condition $P_{S_2}(t = T_2) = \lambda^{R,\mathbf{A}} P_{S_2}(t = T_1)$.

To perform numerical computations, we select a set of Gaussian laser pulses $\varepsilon_a(t)$, centered at different frequencies ω_a:

$$\varepsilon_a(t) = \epsilon_a/(2\sqrt{\pi}\alpha_a) \exp\left(-\left(t/(2\alpha_a)\right)^2 - i\omega_a t\right). \tag{61}$$

The finite-time Fourier transform of this Gaussian pulse, $\varepsilon_a(\omega, t)$, [Eq. (18)], can be expressed analytically [18–20] as:

$$\varepsilon_a(\omega, t) = (\epsilon_a/2) \exp\left(-\alpha_a^2 (\omega - \omega_a)^2\right) \left\{2 - \exp\left[(\alpha_a(\omega - \omega_a) + it/(2\alpha_a))^2\right] W(\alpha_a(\omega - \omega_a) + it/(2\alpha_a))\right\}, \tag{62}$$

where $W(z)$ is the complex error function [20, 21]. At times $t > T_{over} = 4\sqrt{2\ln 2}\,\alpha_a$ this becomes

$$\varepsilon_a(\omega) = \epsilon_a \exp\left(-\alpha_a^2\left(\omega - \omega_a\right)^2\right). \tag{63}$$

Using Eq. (61), the control pulse $\varepsilon_p(t)$ in time domain is

$$\varepsilon_p(t) = \sum_{a=1}^{N_A} d_a \varepsilon_a(t) = \sum_{a=1}^{N_A} d_a \epsilon_a/(2\sqrt{\pi}\alpha_a)\exp\left(-\left(t/(2\alpha_a)\right)^2 - i\omega_a t\right), \tag{64}$$

with infinite-time Fourier transform

$$\varepsilon_p(\omega) = \sum_{a=1}^{N_A} d_a \varepsilon_a(\omega) = \sum_{a=1}^{N_A} d_a \epsilon_a \exp\left(-\alpha_a^2\left(\omega - \omega_a\right)^2\right). \tag{65}$$

By construction, the $\varepsilon_p(\omega_{A,g})$ value should be constant inside the corresponding I_A bin [Eq. (66)]. The $\varepsilon_p(\omega)$ function [Eq. (65)] is smooth and does not satisfy this requirement exactly. Nevertheless, if N_A is large enough each I_A bin becomes relatively small, and the smooth function in Eq. (65) in each bin can be approximately treated as constant.

IV. COMPUTATIONAL RESULTS

Consider $S_0 \to S_2$ excitation to coherently control $S_2 \leftrightarrow S_1$ interconversion dynamics of pyrazine excited using weak light in the perturbative regime. We use the pyrazine vibronic structure of Refs. [7] and [8], and partition the energy into 2000 bins, in the range 4.06–6.06 eV, where energy is referred to the ground vibrational S_0 state. Here, 4.06 eV is the S_1 energy at the S_0 nuclear equilibrium configuration [12, 22]. The Q space consists of the 176 brightest (most optically accessible) $|\kappa\rangle$ resonances, having the largest values of $\langle\kappa|\mu|g\rangle$. In this case the QP-partitioning approach gives 76775 coarse-grained vibronic states $|\overline{\alpha}\rangle$, with energies ranging from 4.06 to 6.06 eV. Thus, there are 76775×176 = 13512400 $R^{\alpha}_{\alpha,\kappa} = \langle\overline{\alpha}|\kappa\rangle$ values. These are used together with 176 $\langle\kappa|\mu|g\rangle$ values to compute the dynamics of interest.

A. Uncontrolled Excitation and Decay Dynamics

Figure 1 shows characteristic examples of $P_{S_2}(t)$ populations produced by a single Gaussian laser pulses of differing time durations, where the subscript u denotes "uncontrolled". These examples are computed with the laser center frequency corresponding to 4.84 eV. It is notable that the uppermost population curve in Fig. 1, produced by the pulse with a time duration ∼1 fs ($\alpha_a = 0.1$ fs) is, at times $t > 0.5$ fs, similar in shape to the zero-zero curve in Fig. 5, Ref. [8]. This is the case because the ultrafast laser pulse behaves like $\epsilon_a\delta(t)$ on the femtosecond timescale, and its finite-time Fourier transform is nearly constant, $\approx \epsilon_a$. As a consequence, in this specific case, after the pulse is over, $P_{S_2}(t)$ in Eq. (31) is the same up to a constant scaling factor as the zero-zero $P_{S_2}(t)$ in Eq. (7), with $c_{\kappa'} \propto (i/\hbar)\langle\kappa'|\mu|g\rangle\epsilon_a$.

Figure 2 shows $P_{S_2}(t)$ populations produced by Gaussian lasers having the same short time duration ≈10 fs ($\alpha_a = 1.0$ fs), but different center frequencies. In this case all populations behave similarly on a short time scale, differing by the overall magnitude due to the difference in $\langle\kappa'|\mu|g\rangle$ values for different resonances $|\kappa'\rangle$.

Figure 3 shows $P_{S_2}(t)$ populations produced by Gaussian lasers with long time duration around 200 fs ($\alpha_a = 20.0$ fs), using different frequencies. In contrast with Fig. 2, there are significant differences in $S_2 \leftrightarrow S_1$ IC dynamics, depending on the frequency used. Figure 3 shows that the laser with 4.84 eV photon energy produces a larger population, which also tends to decay slower, than in other cases, thus, marking the region of relative stability in pyrazine resonance structure.

Both Figs. 2 and 3 qualitatively correlate well with the corresponding results for $S_0 \rightarrow S_2 \leftrightarrow S_1$ dynamics in Ref. [23], obtained using a more general non-perturbative time-dependent dynamical approach [24].

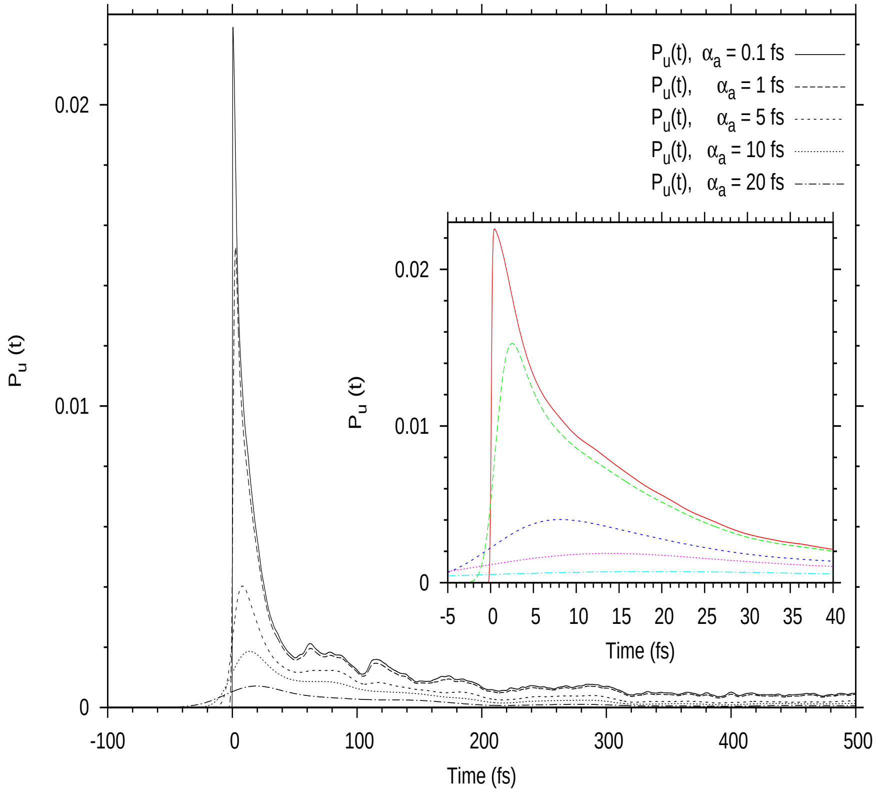

FIG. 1: S_2 populations $P_{S_2}(t)$, denoted $P_u(t)$ here, produced by Gaussian laser pulses of different time duration. Panel inset: The same data, shown on a shorter time scale.

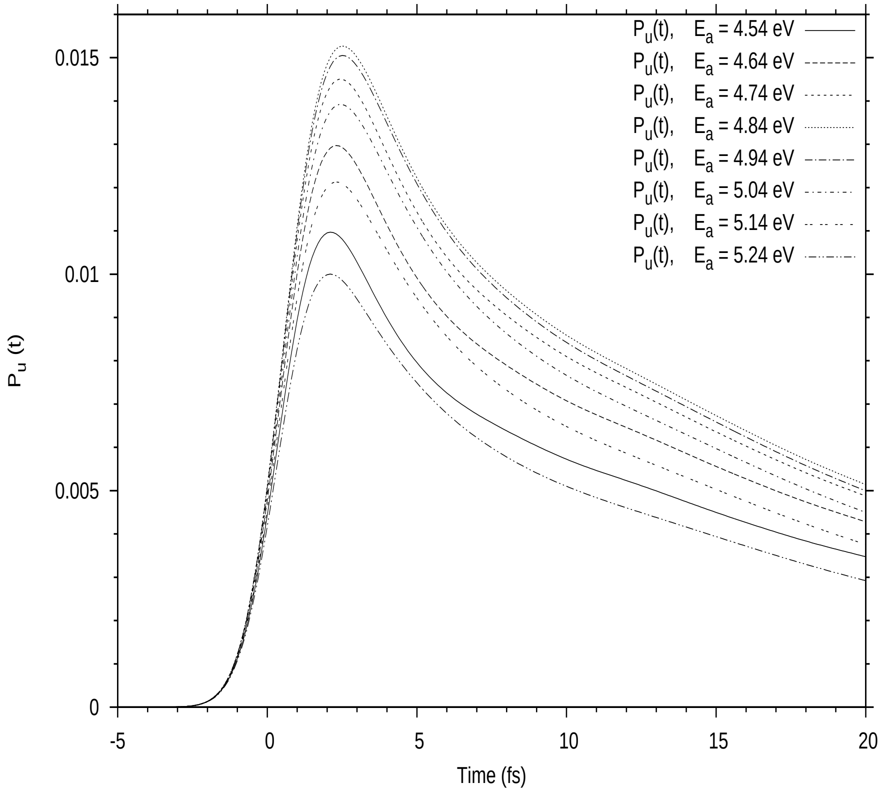

FIG. 2: S_2 populations, $P_{S_2}(t)$, denoted $P_u(t)$ here, produced by short Gaussian laser pulses with the same $\alpha_a = 1.0$ fs, but different center frequencies.

B. Control Involving Multiple Overlapping Resonances

Consider first sample numerical results for $H(\mathbf{\Omega}^\alpha)$, the measure of the extent of resonance overlap [Eq. (54)] and the quantities associated with it. These quantities are $H\left(\mathbf{K}^{\varepsilon,\mathbf{A}}(t)\right)$ [Eq. (48)], which is the $\mathbf{K}^{\varepsilon,\mathbf{A}}(t)$ non-diagonality measure, shown at $T_1 = 150$ fs and $T_2 = 250$ fs; and two measures of the non-diagonality $\mathbf{R}^{\varepsilon,\mathbf{A}}(T_2, T_1)$, $H_R\left(\mathbf{R}^{\varepsilon,\mathbf{A}}(T_2,T_1)\right)$ [Eq. (51)], and $|H_C\left(\mathbf{R}^{\varepsilon,\mathbf{A}}(T_2,T_1)\right)|$ [Eq. (52)]. In addition, we tabulate $\lambda^{R,\mathbf{A}}_{\rm min}$ and $\lambda^{R,\mathbf{A}}_{\rm max}$, denoting minimal and maximal eigenvalues of the eigenproblem in Eq. (46) and which we term "control extents". Values for 128 I_A bins (degrees of freedom of the laser), are listed in Table I. Note first the enormous range of control possible for the ratio $P_{S_2}(T_2)/P_{S_2}(T_1)$ as indicated by the $\lambda^{R,\mathbf{A}}_{\rm min}$ and $\lambda^{R,\mathbf{A}}_{\rm max}$. For example, for the first energy interval, this ratio can range from 3.05×10^{-6} to $3.90 \times 10^{+5}$, a range of over $1 \times 10^{+11}$.

The measures in Table I are obtained using products of 128 matrix elements of the corresponding matrices. Since each of these values is small, we report the 1/128 power of these measures. From Table I one can see a well defined correlation between $H(\mathbf{\Omega}^\alpha)$ and the other quantities. Generally, when $H(\mathbf{\Omega}^\alpha)$ is small, so too are $H\left(\mathbf{K}^{\varepsilon,\mathbf{A}}(T_1)\right)$, $H\left(\mathbf{K}^{\varepsilon,\mathbf{A}}(T_2)\right)$, $H_R\left(\mathbf{R}^{\varepsilon,\mathbf{A}}(T_2,T_1)\right)$ and $|H_C\left(\mathbf{R}^{\varepsilon,\mathbf{A}}(T_2,T_1)\right)|$ (meaning a larger extent of non-diagonality

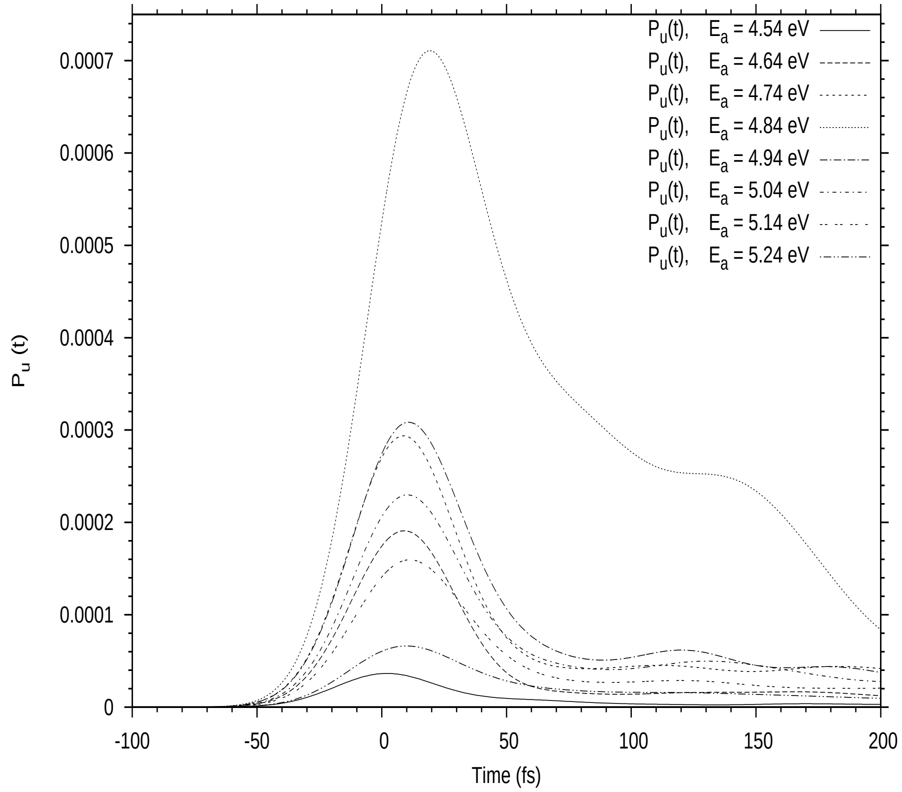

FIG. 3: Bottom: S_2 populations, $P_{S_2}(t)$, denoted $P_u(t)$ here, produced by long Gaussian laser pulses with the same $\alpha_a = 20.0$ fs, but different center frequencies.

TABLE I: The (1/128) power of $H(\boldsymbol{\Omega}^\alpha)$, $H\left(\mathbf{K}^{\varepsilon,\mathbf{A}}(T_1)\right)$, $H\left(\mathbf{K}^{\varepsilon,\mathbf{A}}(T_2)\right)$, $H_R\left(\mathbf{R}^{\varepsilon,\mathbf{A}}(T_2,T_1)\right)$, $|H_C\left(\mathbf{R}^{\varepsilon,\mathbf{A}}(T_2,T_1)\right)|$, as well as $\lambda^{R,\mathbf{A}}_{\rm min}$ and $\lambda^{R,\mathbf{A}}_{\rm max}$ for different energy intervals $[E_L, E_H]$. Here, $T_1 = 150$ fs, $T_2 = 250$ fs.

$[E_L, E_H]$, eV	$[4.46, 4.66]$	$[4.66, 4.86]$	$[4.86, 5.06]$	$[5.06, 5.26]$	$[5.26, 5.46]$
$H(\boldsymbol{\Omega}^\alpha)$	1.76×10^{-1}	2.77×10^{-1}	3.09×10^{-1}	3.15×10^{-1}	2.80×10^{-1}
$H\left(\mathbf{K}^{\varepsilon,\mathbf{A}}(T_1)\right)$	1.08×10^{-2}	2.68×10^{-2}	9.05×10^{-2}	1.36×10^{-1}	1.13×10^{-1}
$H\left(\mathbf{K}^{\varepsilon,\mathbf{A}}(T_2)\right)$	1.23×10^{-2}	2.50×10^{-2}	9.45×10^{-2}	1.29×10^{-1}	1.06×10^{-1}
$H_R\left(\mathbf{R}^{\varepsilon,\mathbf{A}}(T_2,T_1)\right)$	1.41×10^{-4}	8.00×10^{-4}	1.20×10^{-2}	2.38×10^{-2}	1.51×10^{-2}
$\left\vert H_C\left(\mathbf{R}^{\varepsilon,\mathbf{A}}(T_2,T_1)\right)\right\vert$	1.36×10^{-4}	9.05×10^{-4}	1.75×10^{-2}	3.41×10^{-2}	1.79×10^{-2}
$\lambda^{R,\mathbf{A}}_{\rm min}$	3.05×10^{-6}	3.36×10^{-5}	5.54×10^{-4}	1.29×10^{-3}	7.30×10^{-4}
$\lambda^{R,\mathbf{A}}_{\rm max}$	$3.90\times10^{+5}$	$4.32\times10^{+4}$	$1.89\times10^{+3}$	$6.67\times10^{+2}$	$1.92\times10^{+3}$

in the corresponding matrices). In particular, correlation is good with $\lambda^{R,\mathbf{A}}_{\rm max} - \lambda^{R,\mathbf{A}}_{\rm min}$; when it is large, a greater extent of coherent control is possible, in agreement with the non-diagonality measures.

Numerically implementing controlled $P_{S_2}(t)$ dynamics proceeded as follows. First, the eigenvalue problem in Eq. (46) is numerically solved for the particular number of bins N_A in the desired energy range $[E_L, E_H]$, providing the set of eigenvalues $\lambda^{R,\mathbf{A}}$ and corresponding eigenvectors $\underline{\varepsilon}^{\mathbf{A}}$, which give the $\lambda^{R,\mathbf{A}}$ as $P_{S_2}(T_2)/P_{S_2}(T_1)$ ratios during the $P_{S_2}(t)$ time propagation ($T_2 > T_1 \geq T_{over}$). Then, a set of linearly independent N_A Gaussian lasers [Eqs. (61)–(65)], is introduced (all with the same α_a), contiguously and uniformly covering the desired energy range $[E_L, E_H]$. The eigenvectors obtained $\underline{\varepsilon}^{\mathbf{A}}$ are then expanded in terms of this Gaussian basis with the **d** coefficients given by Eq. (57). The dynamics are then propagated from $t \leq -T_{over}$ to $t \geq T_2$ using the corresponding **d** coefficients for each $\underline{\varepsilon}^{\mathbf{A}}$ eigenvector; finite-time Fourier transforms of the pulses in Eq. (58) are produced using Eq. (62), and the pulse time profiles are given in Eq. (64). The perturbative nature of the dynamics makes it possible to scale $P_{S_2}(t)$ uniformly by multiplying the $\underline{\varepsilon}^{\mathbf{A}}$ eigenvector by a scalar constant. We utilized this scaling option to allow presentation of both the maximization and minimization results to be shown on the same figure (upper panel, Fig. 4) below. Specifically, the maximization curve is multiplied throughout by 8.3×10^{-5}

An experimental suggestion of R. J. Gordon (University of Illinois, Chicago) prompted our using a controllable laser in the wavelength range 250–265 nm, with time duration ∼150–200 fs, to study the pyrazine $S_0 \to S_2 \leftrightarrow S_1$ excitation and IC dynamics. Using this as a guide, we computed control and dynamics in the corresponding energy range ($E_L = 4.68$ eV, $E_H = 4.96$ eV), using $T_1 = 150$ fs, $T_2 = 250$ fs, $N_A = 128$, and all $\alpha_a = 21.0$ fs. The resulting S_2 populations, together with resulting control fields in time domain, are shown in Fig. 4 where the subscript c denotes "controlled". Corresponding control fields in the frequency domain are shown in Figs. 5 and 6.

The behavior of the controlled $P_{S_2}(t)$ (Fig. 4), differs in magnitude in the regions when the pulse is acting, and after the pulse is over. To understand this difference, note that to obtain the controlled fields in Figs. 5 and 6 using a set of Gaussians requires that some components of **d** vector be large. After the pulse is over, these components are "balanced" by one another in the *infinite-time* Fourier transform, to give the small desired population value P_0 at $t = T_1$ or $t = T_2$ and to yield the required controlled dynamics. However, while the pulse is acting, these components are "unbalanced" giving large transient $\varepsilon_p(\omega, t)$ values. For similar reasons the controlled pulses, being a linear combinations of single Gaussians, are effectively longer than the single Gaussian pulse (see Fig. 4, lower panel).

To examine the complex structure of the control pulses at Figs. 5 and 6, we apply several approaches to simplify the field while monitoring the control achieved. First, we attempted a local averaging of the controlled field, where the total field in N_A bins is arithmetically averaged (amplitude and phase separately) using a smaller number N_S of larger bins (N_A being an integer multiple of N_S, for example, for $N_A = 64$, $N_S = 32$, 16, 8, 4, 2). By doing so, the resulting averaged field, however, showed virtually no control. Second, this averaged step-like field was expanded with N_S Gaussians and the resulting smoothed field used for the propagation. Again, this case led to nearly complete loss of control.

An alternative simplifying approach was, however, successful. Specifically, we retained only the N_R largest field amplitudes out of the total N_A (with all the smaller ampitudes set to zero), keeping the phase profile intact, and monitoring the changes in control ratios. Sample results for $N_A = 64$ are shown in Fig. 7. A total N_A of 64 is used

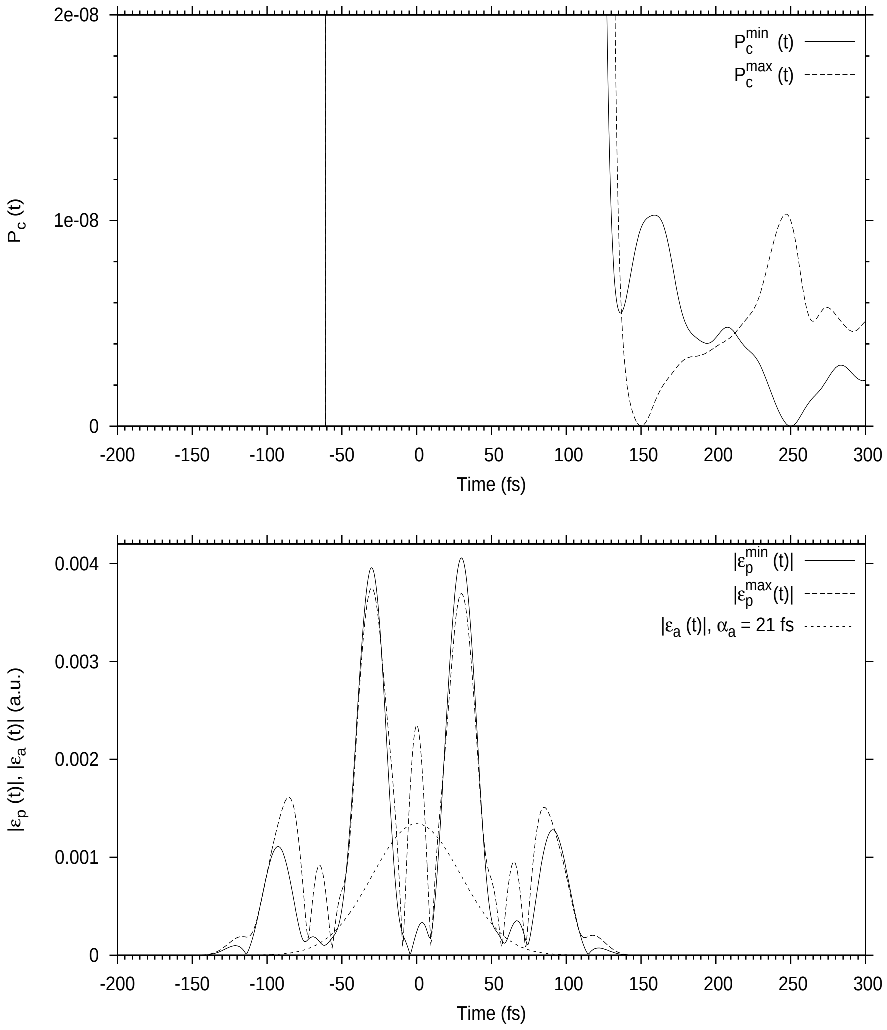

FIG. 4: Upper panel: Two controlled S_2 populations, $P_{S_2}(t)$, denoted $P_c(t)$, which either minimize and maximize $\lambda^{R,\mathbf{A}}$, i.e., the S_2 population ratio at times $T_2 = 250$ fs and $T_1 = 150$ fs. The P_c^{max} curve has been multiplied by 8.3×10^{-5} in order to fit on this figure. Lower panel: Time envelopes of two corresponding controlled laser pulses, $|\varepsilon_p(t)|$, together with the time envelope of the single (uncontrolled) Gaussian laser pulse, $|\varepsilon_a(t)|$.

here (results with $N_A = 128$ are qualitatively the same). It is clear from Fig. 7, that this approach, retaining only the largest amplitudes, works better than the previous two since it tends to partially maintain important dynamical information. Generally, $\lambda_{\min}^{R,\mathbf{A}}$ is more robust with respect to this amplitude truncation than is $\lambda_{\max}^{R,\mathbf{A}}$. Additionally, we found that the extent of control achieved using only N_R amplitudes out of N_A, is similar in magnitude to control extents without truncation, but using this N_R as the original N_A. That is, the same number of degrees of freedom in both cases provides similar extents of control.

Theoretically, maximum and minimum control limits via this approach can be reached using all coarse-grained $|\overline{\alpha}\rangle$ states accessible to the laser, *i.e.*, those belonging to the interval of interest $[E_L, E_H]$. For the case presented in

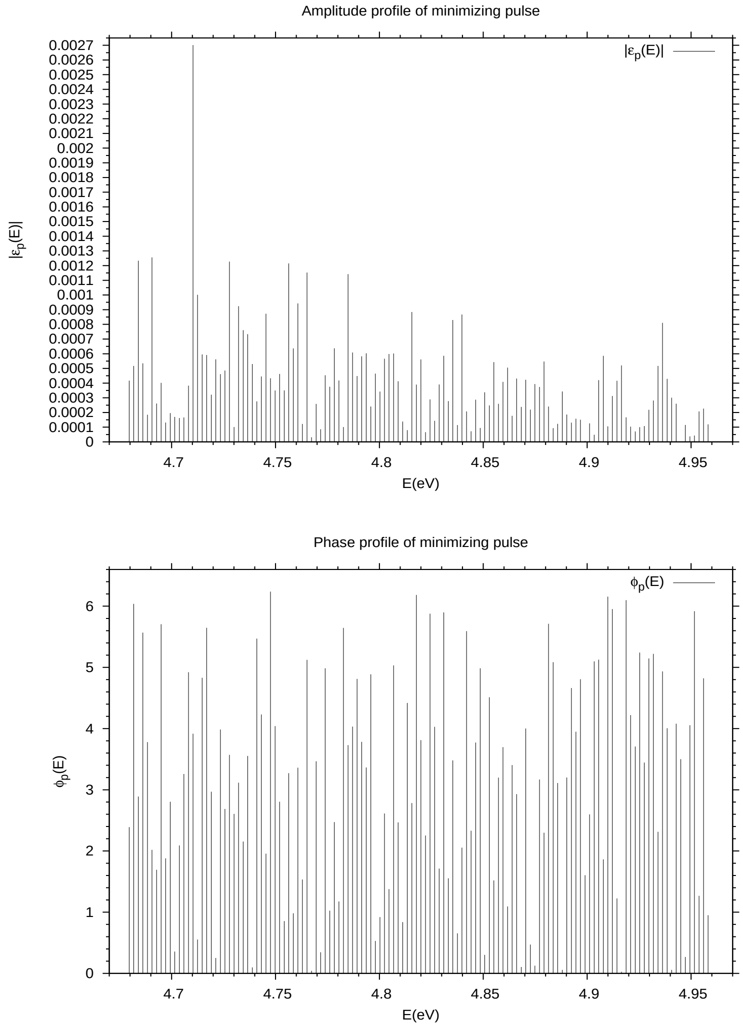

FIG. 5: Amplitude and phase of $\underline{\varepsilon}_p^{\mathbf{A}}$ eigenvector, which minimizes the $P_{S_2}(T_2)/P_{S_2}(T_1)$ ratio. $\lambda_{\min}^{R,\mathbf{A}} = 8.28\times 10^{-5}$.

Figs. 4, 5 and 6, the number of $|\overline{\alpha}\rangle$ states, using our pyrazine description, is 11885. However, as mentioned in the Appendix, the optimization problem for $|\overline{\alpha}\rangle$ states in Eq. (44) is numerically stable only up to dimensionality 150–180, and the control range $\lambda_{\max}^{R,\alpha} - \lambda_{\min}^{R,\alpha}$ continues to increase when the dimensionality increases from 128 to 180, reaching $\sim 10^5$. We anticipate a theoretical control range limit to be $\sim 10^9$–10^{10}, which, however, is not achieved due to the numerical limitations discussed in Appendix (see below).

V. SUMMARY AND CONCLUSIONS

Coherent control of internal conversion (IC) between the first and second singlet excited electronic states of pyrazine (S_1 and S_2) is examined, using two different control objectives. The control is performed by means of shaping the laser, which excites the system from the ground electronic state S_0 to the second excited electronic state

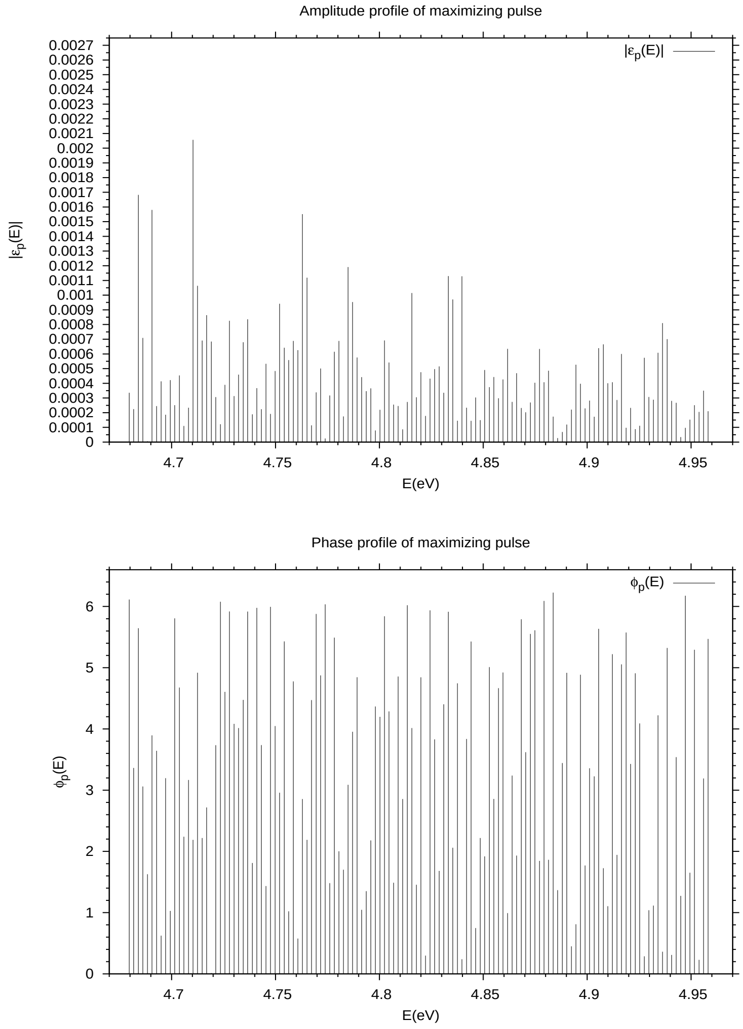

FIG. 6: Amplitude and phase of $\underline{\varepsilon}_p^{\mathbf{A}}$ eigenvector, which maximizes the $P_{S_2}(T_2)/P_{S_2}(T_1)$ ratio. $\lambda^{R,\mathbf{A}}_{\mathrm{max}} = 8.38{\times}10^{+3}$.

S_2. Resonance energy broadening and resonance overlap are shown to be responsible for phase control efficiency, and a correlation between resonance overlap and controllability is established. A huge range of control was obtained for the relative population of S_2 at long times as compared to times just after the pulse is over. Different ways to simplify the controlled fields are described, and the behavior of the control as a consequence of these simplifications is investigated. Specifically, we have found that retaining the largest field amplitudes is the best approach to field simplification.

VI. ACKNOWLEDGEMENTS

This work was supported by the Natural Sciences and Engineering Research Council of Canada (NSERC). This manuscript summarizes one of the last joint efforts of the Brumer and Shapiro research groups. The topic, overlapping resonance effects, was beloved by Moshe. P.B. is grateful for the opportunity to have interacted with such

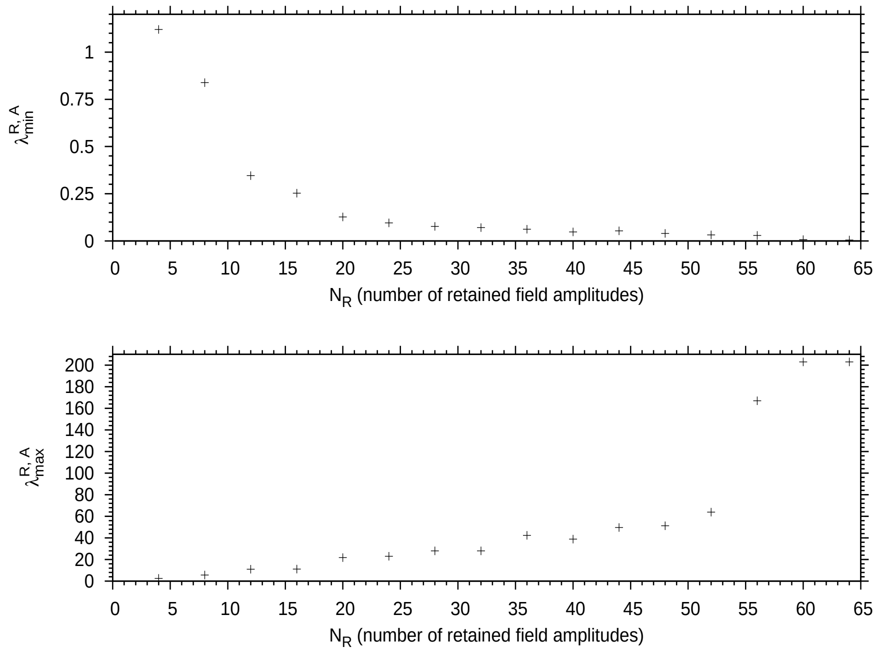

FIG. 7: Upper panel: Dependence of $\lambda_{\rm min}^{R,\mathbf{A}}$ on the number of retained amplitudes N_R. Lower panel: The same, but for $\lambda_{\rm max}^{R,\mathbf{A}}$. Total number of amplitudes $N_A = 64$.

an outstanding scientist for over 40 years, publishing over 120 joint papers, and two books.

---

[1] Current address: Advanced Chemistry Development, Inc., 8 King Street East, Toronto, Ontario, Canada M5C 1B5

[2] S. A. Rice and M. Zhao, *Optical Control of Molecular Dynamics* (Wiley, New York, 2000).

[3] M. Shapiro and P. Brumer, *Principles of the Quantum Control of Molecular Processes* (Wiley, New York, 2003); M. Shapiro and P. Brumer, *Quantum Control of Molecular Processes* (Wiley-VCH, Weinheim, 2012).

[4] E. Frishman and M. Shapiro, Phys. Rev. Lett. **87**, 253001 (2001).

[5] P. S. Christopher, M. Shapiro and P. Brumer, J. Chem. Phys. **126**, 124307 (2007).

[6] P. S. Christopher, M. Shapiro and P. Brumer, J. Chem. Phys. **123**, 064313 (2005).

[7] P. S. Christopher, M. Shapiro and P. Brumer, J. Chem. Phys. **124**, 184107 (2006).

[8] P. S. Christopher, M. Shapiro and P. Brumer, J. Chem. Phys. **125**, 124310 (2006).

[9] R. Borrelli and A. Peluso, J. Chem. Phys. **119**, 8437 (2003).

[10] R. D. Levine, *Quantum Mechanics of Molecular Rate Processes* (Clarendon Press, Oxford, 1969).

[11] M. Shapiro, J. Chem. Phys. **56**, 2582 (1972).

[12] A. Raab, G. A. Worth, H.-D. Meyer and L. S. Cederbaum, J. Chem. Phys. **110**, 936 (1999).

[13] T. Grinev, M. Shapiro and P. Brumer, J. Chem. Phys. **138**, 044306 (2013).

[14] M. Shapiro, J. Phys. Chem. A **102**, *47*, 9570 (1998).

[15] R. He, C. Zhu, C.-H. Chin and S. H. Lin, Chem. Phys. Lett. **476**, 19 (2009).

[16] J. C. Preisig, SIAM J. Control Optim. **34**, 1135 (1996).

[17] R. Kosloff, S. A. Rice, P. Gaspard, S. Tersigni and D. J. Tannor, Chem. Phys. **139**, 201 (1989).

[18] M. Shapiro, J. Phys. Chem. **97**, *29*, 7396 (1993).

[19] M. Shapiro, in *Femtosecond Chemistry*; J. Manz, L. Woste, Eds. (VCH, Weinheim, 1995); p. 321.

[20] E. W. Weisstein, Erf(z) error function. From MathWorld–A Wolfram Web Resource. http://mathworld.wolfram.com/Erf.html

[21] M. Abramowitz and I. A. Stegun, *Handbook of Mathematical Functions* (Dover, New York, 1965); Eqs. 7.1.3 and 7.1.8.

[22] X. Chen and V. S. Batista, J. Chem. Phys. **125**, 124313 (2006).

[23] I. Thanopulos, X. Li, P. Brumer and M. Shapiro, J. Chem. Phys. **137**, 064111 2012.

[24] I. Thanopulos, P. Brumer and M. Shapiro, J. Chem. Phys. **133**, 154111 (2010).

Appendix: Energy Partitioning for Control Associated with Overlapping Resonances

As noted in Sect. III B, numerical instabilities necessitated that we introduce a further partitioning of the energy axis. Specifically, we partitioned the energy axis into a limited number of N_A bins in Eq. (27):

$$\begin{aligned}\langle\kappa|\Psi_p(t)\rangle &\approx \sum_A \sum_{\alpha\in I_A} \varepsilon_p(\omega_{\alpha,g},t) M^{\varepsilon,\alpha}_{\kappa,\alpha}(t) \\ &\approx \sum_A \varepsilon_p(\omega_{A,g},t)\left[\sum_{\alpha\in I_A} M^{\varepsilon,\alpha}_{\kappa,\alpha}(t)\right] \equiv \sum_A \varepsilon_p(\omega_{A,g},t) M^{\varepsilon,\mathbf{A}}_{\kappa,A}(t),\end{aligned} \tag{66}$$

where I_A is a bin number A, which has the center energy E_A, $\omega_{A,g}\equiv(E_A-E_g)/\hbar$, and

$$M^{\varepsilon,\mathbf{A}}_{\kappa,A}(t) \equiv \sum_{\alpha\in I_A} M^{\varepsilon,\alpha}_{\kappa,\alpha}(t) \tag{67}$$

is the collective material system matrix element, corresponding to bin I_A. Here and below, the bold superscript **A** denotes that all the corresponding quantities are written for $|A\rangle$ states, which are defined below.

Using Eq. (28), $M^{\varepsilon,\mathbf{A}}_{\kappa,A}(t)$ can be written as:

$$M^{\varepsilon,\mathbf{A}}_{\kappa,A}(t) = \sum_{\alpha\in I_A} \langle\kappa|\overline{\alpha}\rangle\, \tau_\alpha(t)\, \frac{i}{\hbar} \sum_{\kappa'} \langle\overline{\alpha}|\kappa'\rangle\langle\kappa'|\mu|g\rangle \equiv \langle\kappa| \left[\sum_{\alpha\in I_A} \tau_\alpha(t)|\overline{\alpha}\rangle\langle\overline{\alpha}|\right] \left[\sum_{\kappa'} \frac{i}{\hbar}\langle\kappa'|\mu|g\rangle|\kappa'\rangle\right]. \tag{68}$$

The middle expression in square brackets, unlike Eq. (28), is not the single $|\overline{\alpha}\rangle$ state propagator, but the localized coarse-grained propagator, with the sum only over $|\overline{\alpha}\rangle$ states belonging to the bin I_A.

One can introduce the “binned” states $|A\rangle$, such that the corresponding projector onto the state $|A\rangle$ is

$$|A\rangle\langle A| = (1/N_{I_A}) \sum_{\alpha\in I_A} |\overline{\alpha}\rangle\langle\overline{\alpha}|, \quad \text{hence} \quad \sqrt{N_{I_A}}|A\rangle\langle A|\sqrt{N_{I_A}} = \sum_{\alpha\in I_A} |\overline{\alpha}\rangle\langle\overline{\alpha}|,$$

where N_{I_A} is the number of $|\overline{\alpha}\rangle$ states that are inside bin I_A. With the notation $|\overline{A}\rangle \equiv \sqrt{N_{I_A}}|A\rangle$ we have

$$|\overline{A}\rangle\langle\overline{A}| = \sum_{\alpha\in I_A} |\overline{\alpha}\rangle\langle\overline{\alpha}|. \tag{69}$$

Using Eq. (69), the propagator in Eq. (68) can be approximately rewritten as:

$$\sum_{\alpha\in I_A} \tau_\alpha(t)|\overline{\alpha}\rangle\langle\overline{\alpha}| \approx |A\rangle\langle A| \sum_{\alpha\in I_A} \tau_\alpha(t) \equiv \tau^{\mathbf{A}}_A(t)|\overline{A}\rangle\langle\overline{A}|, \tag{70}$$

where $\tau^{\mathbf{A}}_A(t) \equiv (1/N_{I_A})\sum_{\alpha\in I_A}\tau_\alpha(t)$. The accuracy of the approximation made in Eq. (70) rapidly increases with decreasing bin size. Using Eq. (70), $M^{\varepsilon,\mathbf{A}}_{\kappa,A}(t)$ in Eq. (68) can be rewritten as:

$$M^{\varepsilon,\mathbf{A}}_{\kappa,A}(t) \approx \langle\kappa|\overline{A}\rangle \tau^{\mathbf{A}}_A(t) \frac{i}{\hbar} \sum_{\kappa'} \langle\overline{A}|\kappa'\rangle\langle\kappa'|\mu|g\rangle. \tag{71}$$

Defining

$$\mu^{\mathbf{A}}_A \equiv \frac{i}{\hbar}\sum_{\kappa'}\langle\overline{A}|\kappa'\rangle\langle\kappa'|\mu|g\rangle = \frac{i}{\hbar}\langle\overline{A}|\mu|g\rangle, \qquad R^{\mathbf{A}}_{A,\kappa} \equiv \langle\overline{A}|\kappa\rangle \tag{72}$$

gives

$$\mathbf{M}^{\varepsilon,\mathbf{A}}(t) = \mathbf{R}^{\mathbf{A}\dagger}\,\underline{\underline{\tau}}^{\mathbf{A}}(t)\,\underline{\underline{\mu}}^{\mathbf{A}}, \qquad \mathbf{K}^{\varepsilon,\mathbf{A}}(t) = \mathbf{M}^{\varepsilon,\mathbf{A}\dagger}(t)\mathbf{M}^{\varepsilon,\mathbf{A}}(t) = \underline{\underline{\mu}}^{\mathbf{A}\dagger}\underline{\underline{\tau}}^{\mathbf{A}\dagger}(t)\mathbf{R}^{\mathbf{A}}\mathbf{R}^{\mathbf{A}\dagger}\,\underline{\underline{\tau}}^{\mathbf{A}}(t)\,\underline{\underline{\mu}}^{\mathbf{A}}, \tag{73}$$

where $\underline{\underline{\tau}}^{\mathbf{A}}(t)$ is a square diagonal matrix composed of $\tau_A^{\mathbf{A}}(t)$ values, and $\underline{\underline{\mu}}^{\mathbf{A}}$ is a square diagonal matrix composed of $(i/\hbar)\langle\overline{A}|\mu|g\rangle$ values. This gives the $P_{S_2}(t)$ population in terms of binned values as

$$P_{S_2}(t) = \underline{\varepsilon}^{\mathbf{A}\dagger}(t)\underline{\underline{\mu}}^{\mathbf{A}\dagger}\underline{\underline{\tau}}^{\mathbf{A}\dagger}(t)\mathbf{R}^{\mathbf{A}}\mathbf{R}^{\mathbf{A}\dagger}\,\underline{\underline{\tau}}^{\mathbf{A}}(t)\,\underline{\underline{\mu}}^{\mathbf{A}}\underline{\varepsilon}^{\mathbf{A}}(t) \tag{74}$$

$$= \sum_{A'} |\varepsilon_p(\omega_{A',g},t)|^2 K^{\varepsilon,\mathbf{A}}_{A',A'}(t) + \sum_{A'\neq A''} \varepsilon_p^*(\omega_{A',g},t)\varepsilon_p(\omega_{A'',g},t)K^{\varepsilon,\mathbf{A}}_{A',A''}(t), \tag{75}$$

where $\underline{\varepsilon}^{\mathbf{A}}(t)$ is a vector composed of $\varepsilon_p(\omega_{A,g},t)$ components.

Since $\underline{\underline{\mu}}^{\mathbf{A}}$ and $\underline{\underline{\tau}}^{\mathbf{A}}(t)$ are diagonal, the only possible source of nondiagonality in Eq. (73) for $\mathbf{K}^{\varepsilon,\mathbf{A}}(t)$ and Eq. (75) is $\mathbf{Q}^{\mathbf{A}} = \mathbf{R}^{\mathbf{A}}\mathbf{R}^{\mathbf{A}\dagger}$, composed of $Q^{\mathbf{A}}_{A',A''} = \langle\overline{A}'|Q|\overline{A}''\rangle$ values. Thus, the possibility of phase control by means of phases $\phi_A(t)$ of complex $\varepsilon_p(\omega_{A,g},t) = |\varepsilon_p(\omega_{A,g},t)|\exp(i\phi_A(t))$ depends solely on its properties. As in the previous case of $|\gamma\rangle$ and $|\overline{\alpha}\rangle$, all the $P_{S_2}(t)$ phase control considerations remain the same, except that $|\gamma\rangle$ or $|\overline{\alpha}\rangle$ states are replaced by $|\overline{A}\rangle$ states. Namely, phase control is provided by resonance energy broadening and resonance overlap. The resonance overlap effect, providing the non-block-diagonal structure of $\mathbf{Q}^{\mathbf{A}}$ and $\mathbf{K}^{\varepsilon,\mathbf{A}}(t)$ as a consequence, enhances the effect of resonance broadening.

Using Eq. (75), the eigenproblem in Eq. (44) is reformulated as

$$\mathbf{R}^{\varepsilon,\mathbf{A}}(T_2,T_1)\underline{\varepsilon}^{\mathbf{A}} = \lambda^{R,\mathbf{A}}\underline{\varepsilon}^{\mathbf{A}}, \tag{76}$$

$$\mathbf{R}^{\varepsilon,\mathbf{A}}(T_2,T_1) \equiv [\mathbf{K}^{\varepsilon,\mathbf{A}}(T_1)]^{-1}\mathbf{K}^{\varepsilon,\mathbf{A}}(T_2). \tag{77}$$

Its dimensionality reduced from N_α to N_A, allowing an accurate numerical solution for N_A values up to 150-180.